ELSEVIER

International Journal of Mass Spectrometry 185/186/187 (1999) 155–163

International Journal of Mass Spectrometry

Unimolecular reaction dynamics from kinetic energy release distributions. IV. Dissociation of the pyridine ion

P. Urbain, B. Leyh[1], F. Remacle[1], J.C. Lorquet*

Département de Chimie, Université de Liège, Sart-Tilman, B-4000 Liège 1, Belgium

Received 19 May 1998; accepted 3 July 1998

Abstract

The kinetic energy release distribution (KERD) for the dissociation of the pyridine ion into $C_4H_4^{\cdot+}$ + HCN in the microsecond time window has been experimentally determined and theoretically analyzed by the maximum entropy method. Less energy is channeled into the reaction coordinate than the statistical estimate because of the action of the "momentum gap law." The larger the value of the relative translational momentum of the fragments, the less efficient the exploration of phase space. The fraction of phase space effectively sampled is estimated to be of the order of 75%. (Int J Mass Spectrom 185/186/187 (1999) 155–163) © 1999 Elsevier Science B.V.

Keywords: Kinetic energy release; Pyridine ion; Validity of statistical theory; Maximum entropy method; Phase space

1. Introduction

For many years, mass spectrometrists have tried to extract information from a study of the translational energy released on the dissociation fragments of a unimolecular reaction. Experimentation provides a function called the kinetic energy release distribution (KERD), which expresses the probability $P(\varepsilon|E)$ that an ion of internal energy E releases when it dissociates a translational kinetic energy ε. E is defined as the energy in excess of the thermochemical threshold. Several models have been proposed, including the important contribution developed by Professor Michael T. Bowers to whom we are pleased to dedicate the present article. These methods have been reviewed recently by Baer and Hase [1].

The crudest approximation is that provided by the Rice–Ramsperger–Kassel–Marcus (RRKM) theory. Let us assume the absence of any reverse activation barrier along the reaction path. Assume furthermore that no redistribution of energy takes place beyond the transition state. Then, the distribution is given by [1, 2]:

$$P(\varepsilon|E) = N^*(E-\varepsilon)\Big/\int_0^E N^*(E-\varepsilon)d\varepsilon \qquad (1)$$

where $N^*(E)$ is the density of states of the transition state.

The crux of the matter concerns the behaviour of the KERD around $\varepsilon = 0$. In the RRKM-QET (quasi-equilibrium theory) model, it undergoes a sharp discontinuity at the origin. The problem is taken care of in other theories, which all include conservation of

* Corresponding author.

[1] Chercheur qualifié du F.N.R.S. (Belgium).

Dedicated to Professor Michael T. Bowers on the occasion of his 60th birthday.

PII S1387-3806(98)14080-0

angular momentum, developed by Klots [3–7], Chesnavich and Bowers [8, 9], and by Quack and Troe [10]: phase space theory, orbiting transition state theory, and a statistical adiabatic channel model.

The present article is based on a different approach, denoted surprisal theory and maximum entropy method [11–16]. It has already been applied in the past to study KERDs of ions [17–20], and is briefly summarized in the following section.

After a thorough study of the dissociation of the halogenobenzene cations [21,22] where, essentially, a simple bond breaking and a loose transition state are involved, we chose to apply this method to a presumably more complicated dissociation process, the loss of HCN from the pyridine cation.

2. Maximum entropy formalism

Any nonstatistical effect in a chemical reaction is a consequence of the existence of dynamical constraints that prevent uniform exploration of phase space before dissociation. The purpose of an analysis by the maximum entropy formalism [11–15] is to identify these constraints. The latter can result, e.g. from conservation of linear and angular momenta, from inefficient coupling among oscillators, and from exit-channel interactions, i.e. from conversion of translational into rovibrational energy as the fragments separate. Briefly, the analysis starts from the so-called prior distribution $P^0(\varepsilon|E)$, which represents the most statistical situation, i.e. the (hypothetical) KERD that would have been measured in the case of totally unconstrained dynamics. The maximum entropy method provides the relationship between this prior distribution and the most probable distribution (i.e. the one of maximum entropy) compatible with the available experimental information at our disposal.

The prior distribution is given by [1,11–15,23]:

$$P^0(\varepsilon|E) = N_{\mathrm{tr}}(\varepsilon)\, N(E-\varepsilon) \Big/ \int_0^E N_{\mathrm{tr}}(\varepsilon)\, N(E-\varepsilon)\, d\varepsilon \equiv A(E)\sqrt{\varepsilon}\, N(E-\varepsilon) \quad (2)$$

where $N(E-\varepsilon)$ now denotes the density of rovibrational states of the two fragments and $N_{\mathrm{tr}}(\varepsilon)$ is the three-dimensional translational density of states, proportional to $\sqrt{\varepsilon}$.

Just as in phase space theory, the prior distribution assumes that all the quantum states of the products are populated with equal probability. However, the conservation of the total angular momentum is not included in our treatment because this requires some prior knowledge about the reaction mechanism [12, 24]. Therefore, $P^0(\varepsilon|E)$ is calculated subject to energy conservation only, with a three-dimensional density of translational states. In this respect, it is important to note that the prior distribution should not be regarded as providing a cheap, rapid, and often inaccurate approximation to the experimentally observed distribution. It should not be "made more realistic" or "converted into a more correct distribution" [1] by reducing the number of translational or rotational degrees of freedom to account for conservation of linear and angular momentum. The basic idea of the maximum entropy method is not to calculate a prior distribution that best describes the experimental situation, but rather to extract information from a comparison of the experimental distribution with a *reference* state [12]. In other words, $P^0(\varepsilon|E)$ describes the situation of maximum entropy, obtained if the distribution were determined by statistics (state counting) alone. Any deviation with respect to the prior distribution indicates the operation of dynamical factors, denoted constraints, which results in a situation of lesser entropy, i.e. in incomplete phase space sampling. The deviation is measured by the so-called entropy deficiency denoted DS. It can be shown [25,26] that the quantity $\exp(-DS)$ represents the fraction of phase space actually sampled by the reaction products, i.e. in our case, by the dissociation fragments. This measurement of the extent of phase space sampling is related to the validity of statistical theories.

It turns out that the relationship between the experimentally determined distribution $P(\varepsilon|E)$ and the prior distribution is often quite simple. For example, we have previously studied the halogen loss reaction from the halogenobenzene ions [21,22]:

$$C_6H_5X^{\cdot+} \rightarrow C_6H_5^+ + X^{\cdot} \quad (3)$$

In that case, the KERD was found to obey the following equation:

$$P(\varepsilon|E) = P^0(\varepsilon|E)\exp(-\lambda_0)\exp(-\lambda_1\sqrt{\varepsilon}) \quad (4)$$

The quantity $\varepsilon^{1/2}$ is therefore called *the informative variable* or, briefly, the *constraint*. Its presence indicates that the internal dynamics is indeed constrained by the square root of the relative translational energy of the separating fragments, i.e. by their momentum. This can be related to the so-called momentum gap law, as will be discussed in Sec. 5.

In the general case, several constraints may have to be taken into account. The distribution $P(\varepsilon|E)$ of maximal entropy can then be shown to be related to the prior distribution [Eq. (2)] in the following way [11–15]:

$$P(\varepsilon|E) = P^0(\varepsilon|E)\exp\left(-\lambda_0 - \sum_{r=1}^{n} \lambda_r A_r\right) \quad (5)$$

The λ_r are Lagrange parameters and the A_r are the n constraints. This functional form ensures that $P(\varepsilon|E)$ is normalized, reproduces the average value $\langle A_r\rangle$ of the constraints obtained from the experimental distribution,

$$\langle A_r\rangle = \int_0^E P(\varepsilon|E)\,A_r\,d\varepsilon \quad (6)$$

and is otherwise of maximum entropy.

The decisive advantage of the maximum entropy method is that the functional form of the constraints can be given a physical significance. A different set of constraints implies a difference in the reaction mechanism.

A related way of comparing the information contained in the experimental distribution $P(\varepsilon|E)$ with the prior distribution $P^0(\varepsilon|E)$ is to consider the surprisal I:

$$I(\varepsilon|E) = -\ln\left(\frac{P(\varepsilon|E)}{P^0(\varepsilon|E)}\right) = \lambda_0 + \sum_{r=1}^{n} \lambda_r A_r \quad (7)$$

When integrated over the experimental distribution $P(\varepsilon|E)$, the previous equation generates the opposite of the entropy deficiency DS:

$$DS(E) = \int_0^E P(\varepsilon|E)\,\ln\left(\frac{P(\varepsilon|E)}{P^0(\varepsilon|E)}\right)d\varepsilon$$

$$= -\lambda_0 - \sum_{r=1}^{n} \lambda_r\langle A_r\rangle \quad (8)$$

The entropy deficiency is the difference between the entropy of the actual distribution $P(\varepsilon|E)$, denoted S, and that of the prior, denoted S^0:

$$DS(E) = S^0(E) - S(E) \quad (9)$$

By definition, the entropy S^0 of the prior distribution is equal to or greater than the entropy S of the experimental distribution, so that the entropy deficiency DS is always equal to zero or positive.

The fraction of phase space actually sampled during the dynamics is given by [25,26]

$$F = \exp(-DS) \quad (10)$$

A value of F equal to unity corresponds to a case of unconstrained dynamics. The prior and the experimental distributions coincide, so that the entropy deficiency, DS, is equal to zero. In all other cases, $F < 1$.

3. Experiment

The KERDs for the $C_5H_5N^{\cdot+} \rightarrow C_4H_4^{\cdot+}$ + HCN reaction are deduced from two types of ion kinetic energy spectra recorded with a forward geometry AEI-MS9 mass spectrometer. Both the accelerating voltage scan method [27] and the scanning of the magnet [28] were used. The first scanning method allows us to observe dissociations taking place in the first field-free region (between the ion source exit slit and the electrostatic analyzer) whereas in the second one dissociations taking place in the second field-free region (between the electrostatic analyzer and the magnet) are monitored.

Table 1
Time window and most probable internal energy E_s, first moments of the KERDs, and values of λ_1, DS, and e^{-DS} (at $E = E_S$) obtained for the metastable decomposition $C_5H_5N^{\cdot+} \rightarrow C_4H_4^{+} + HCN$. For experiments in the first field-free region (1 FFR), the translational energy of $C_4H_4^+$ in the laboratory frame is mentioned. For those in the second field-free region (2 FFR), the electron impact energy V_e is reported. Experiments in the second field-free region have been conducted with an accelerating voltage of 8 keV. The relative uncertainty on the average KER $\langle\varepsilon\rangle$ is estimated to be of the order of ±3%. The uncertainty on e^{-DS} is equal to ±0.03.

	2 FFR V_e = 20.8 eV	2 FFR V_e = 70 eV	1 FFR (1 keV)	1 FFR (3 keV)	1 FFR (5 keV)
τ_1 (μs)	8.06	8.06	1.95	1.49	1.27
τ_2 (μs)	10.92	10.92	5.28	3.42	2.76
E_s (eV)	0.64	0.64	0.80	0.86	0.90
k_{opt} (10^5 s^{-1})	1.1	1.1	3.0	4.3	5.2
ν	4.7	4.7	4.8	4.8	4.8
$\langle\varepsilon\rangle$ (eV)	0.048	0.050	0.070	0.056	0.059
$\langle\varepsilon^2\rangle$ (eV^2)	0.0042	0.0044	0.0110	0.0057	0.0063
λ_1 ($eV^{-1/2}$)	7.5	7.0	6.5	7.5	7.2
DS	0.29	0.26	0.32	0.35	0.33
e^{-DS}	0.75	0.77	0.73	0.71	0.72

The kinetic energy released on the fragments during the dissociations broadens the ion signal, which is measured in the laboratory frame. In the present study, the instrumental broadening as well as y- and z-discrimination can be neglected (see discussion in [21]), so that the KERDs in the centre-of-mass frame can be obtained by numerical differentiation of the measured ion kinetic energy spectrum followed by a transformation of variables from the laboratory coordinates to the centre-of-mass coordinates [29–31]. The differentiation has been done using the Holmes–Osborne procedure [29]. The electrostatic analyzer exit slit (β-slit) has been closed to 0.25 mm to reach an energy resolution $\Delta E/E$ of 10^{-3}, which makes any deconvolution procedure unnecessary.

Our experiments sample dissociations that occur in a time window defined by the entry and exit times in the field-free region, denoted τ_1 and τ_2. The corresponding transmission function T depends on the rate constant of the dissociation that, in turn, depends on the internal energy of the molecular ion E:

$$T[k(E)] = B\{\exp[-k(E)\tau_1] - \exp[-k(E)\tau_2]\} \quad (11)$$

B is a normalization factor.

This means that the dissociating ions sampled are characterized by an internal energy distribution corresponding to the $T(E)$ function. As a result, the KERD $\tilde{P}(\varepsilon)$ effectively measured in actual experiments is an average over this function:

$$\tilde{P}(\varepsilon) = \int_{\varepsilon}^{\infty} P(\varepsilon|E)T(E)dE \quad (12)$$

In the internal energy range covered by $T(E)$, the rate constant $k(E)$ has been fitted to the following empirical form, using literature values [32–34]

$$k(E) = k_{opt}(E/E_s)^{\nu} \quad (13)$$

$T(E)$ reaches its maximum at an energy denoted E_s where k is equal to k_{opt}. Table 1 gives the value of k_{opt}, E_s and ν obtained for the different experimental conditions described below.

In order to shift the time window and thus the distribution $T(E)$ sampled in our experiments, we have varied the times τ_1 and τ_2 in two different ways: (1) first, by working at three different translational energies of the fragment ion in the laboratory frame, and (2) by using both field-free regions of the mass spectrometer. The corresponding transmission functions are displayed in Fig. 1.

Accelerating voltage scan spectra have been recorded for fragment ion translational energies equal to 1, 3, and 4 keV (in the laboratory frame). Magnet scan spectra have been measured with an acceleration voltage equal to 8 kV. The following ion source conditions were applied. Trap current: 30 μA. Electron energy: 70 eV, except for some magnet scan spectra for which the electron energy (V_e) has been

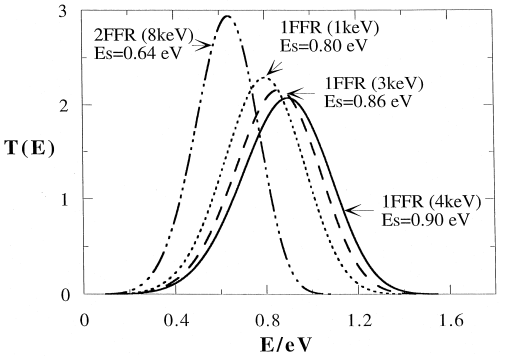

Fig. 1. Collection efficiency $T(E)$ [Eq. (11)] for the metastable dissociations $C_5H_5N^{\cdot+} \rightarrow C_4H_4^{\cdot+}$ + HCN taking place in the first and in the second field-free regions of the AEI-MS9 mass spectrometer. For the dissociations taking place in the first field-free region, the experiments have been carried out at various translational energies (in the laboratory frame).

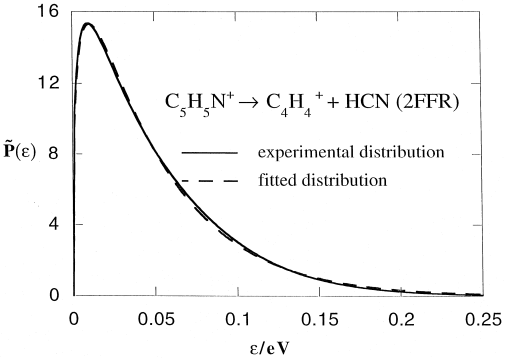

Fig. 2. Experimental KERD $\tilde{P}(\varepsilon)$ and fit to Eq. (17) for the metastable dissociation $C_5H_5N^{\cdot+}$ (8 keV) $\rightarrow C_4H_4^{\cdot+}$ + HCN taking place in the second field-free region. In this spectrum, ionization resulted from 70 eV electron impact.

reduced to 20.8 eV in order to eliminate overlap with more intense signals coming from fragment ions produced in the ion source. Ion source pressure (measured at an ion gauge located approximately 15 cm from the ionization chamber): 10^{-4} Pa. Pyridine provided by Union Chimique Belge (UCB) (purity for analysis, >99%) was carefully degassed but otherwise used without further purification.

4. Results

4.1. Surprisal analysis

The main results concerning the distributions obtained under the various experimental conditions described in the previous section are summarized in Table 1. In particular, this table mentions the values of the first few moments of the distributions. As an example, the distribution obtained for the dissociation $C_5H_5N^{\cdot+}$ (8 keV) $\rightarrow C_4H_4^{\cdot+}$ + HCN, taking place in the second field-free region, is presented in Fig. 2.

In view of the very simple form of the experimental kinetic energy distributions $\tilde{P}(\varepsilon)$ (Fig. 2), it was reasonable to introduce a single constraint A_1 in the maximum entropy method, as was done in the case of the halogenobenzene ions [21, 22]. Then, Eq. (5) becomes

$$P(\varepsilon|E) = P^0(\varepsilon|E)\exp(-\lambda_0 - \lambda_1 A_1) \tag{14}$$

Therefore, once the appropriate constraint A_1 has been identified, the surprisal I (Eq. 7) is linear with respect to A_1.

Since our experiments do not generate $P(\varepsilon|E)$ for a single internal energy E but an average over the transmission function $T(E)$, $\tilde{P}(\varepsilon)$ [Eq. (12)], an average surprisal was introduced:

$$\tilde{I} = -\ln[\tilde{P}(\varepsilon)/\tilde{P}^0(\varepsilon)] \tag{15}$$

where $\tilde{P}(\varepsilon)$ is the actual experimental distribution plotted in solid lines in Fig. 2 and

$$\tilde{P}^0(\varepsilon) = \int_{\varepsilon}^{\infty} P^0(\varepsilon|E)T(E)dE \tag{16}$$

The prior distribution $P^0(\varepsilon|E)$ has been calculated according to Eq. (2). The density of internal states $N(E)$ was calculated with a Beyer–Swinehardt algorithm [35]. Rotational parameters and vibrational frequencies for the $C_4H_4^{\cdot+}$ ion, assuming a methylenecyclopropene structure [36–43], were calculated ab initio at the HF/6-31G* level using the GAUSSIAN 94 set of programs [44].

The average quantity $\tilde{I}$ plays an important role in the determination of the functional form of the constraint: a linear variation of $\tilde{I}$ with respect to the selected constraint is a good indication of its rele-

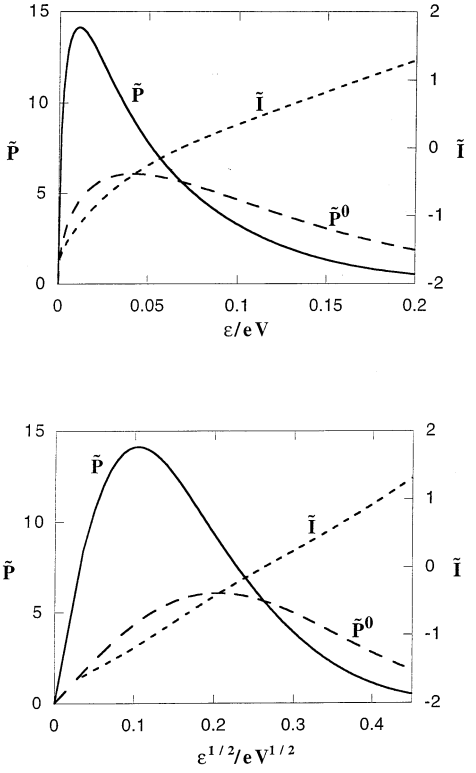

Fig. 3. Average surprisal $\tilde{I}$ plotted as a function of ε (top) and $\varepsilon^{1/2}$ (bottom) for the reaction $C_5H_5N^{\cdot+} \rightarrow C_4H_4^{\cdot+}$ (4 keV) + HCN (1 FFR). The actual $[\tilde{P}(\varepsilon)]$ and prior $[\tilde{P}^0(\varepsilon)]$ distributions, as defined in Eqs. (12) and (16), are also displayed.

vance. $\tilde{I}$ is plotted as a function of ε and of $\varepsilon^{1/2}$ for the reaction $C_5H_5N^{\cdot+} \rightarrow C_4H_4^{\cdot+}$ (4 keV) + HCN (1 FFR) in Fig. 3.

The analysis of Fig. 3 shows that $\tilde{I}$ varies in a fairly linear way when plotted as a function of $\varepsilon^{1/2}$ but not when plotted as a function of ε. Similar results have been obtained for the experiments carried out at 1 and 3 kV and in the second field-free region (Fig. 4). Two conclusions can be derived. First, the dynamics are dominated by a single constraint that can be identified as the translational momentum of the separating fragments. Second, the Lagrange parameter λ_1 can be expected to remain constant in the energy range sampled by the function $T(E)$.

It follows that Eq. (4) should here also describe the KERD, as in the case of the halogenobenzene family.

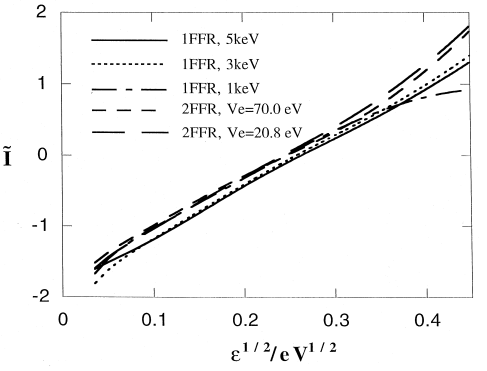

Fig. 4. Average surprisal $\tilde{I}$ plotted as a function of $\varepsilon^{1/2}$ for the metastable dissociations $C_5H_5N^{\cdot+} \rightarrow C_4H_4^{\cdot+}$ + HCN taking place in the first and in the second field-free regions.

4.2. Kinetic energy distribution

The next step consists of fitting the observed KERD to the functional form predicted by the maximum entropy method, which results from the substitution of Eq. (4) into Eq. (12):

$$\tilde{P}(\varepsilon) = \int_{\varepsilon}^{\infty} T(E)\, P^0(\varepsilon|E) \exp(-\lambda_0 - \lambda_1 \varepsilon^{1/2}) dE$$

$$= \int_{\varepsilon}^{\infty} dE\, \frac{T(E)\varepsilon^{1/2} N(E-\varepsilon)\exp(-\lambda_1 \varepsilon^{1/2})}{C(E)} \tag{17}$$

with

$$C(E) = \frac{\exp(\lambda_0)}{A(E)}$$

$$= \int_0^E d\varepsilon\ \varepsilon^{1/2} \exp(-\lambda_1 \varepsilon^{1/2})\, N(E-\varepsilon) \tag{18}$$

Fig. 2 shows that Eq. (17) leads to a very good least squares fit to the experimental data obtained for the pyridine ion in the second field-free region (V_e = 70 eV). Similar results, reported in Table 1, have been obtained for the other experimental conditions. These fits, together with the surprisal analysis (Figs. 3 and 4), confirm that the dynamics are dominated by a

single constraint, $\varepsilon^{1/2}$, bearing on the momentum of the separating fragments.

4.3. Entropy deficiency

The entropy deficiency that corresponds to our kinetic energy distributions at a given internal energy has the following form [Eq. (8)]:

$$DS = S^0 - S = -\lambda_0 - \lambda_1\langle\varepsilon^{1/2}\rangle \quad (19)$$

where $\langle\varepsilon^{1/2}\rangle$ is the average of the constraint $\varepsilon^{1/2}$ on the kinetic energy distribution.

The values obtained for DS and e^{-DS} at $E = E_s$ for the five time windows investigated are presented in Table 1. The entropy deficiency e^{-DS} measures the fraction of phase space sampled by the pair of fragments with respect to the statistical value. Values of the order of 75% are obtained.

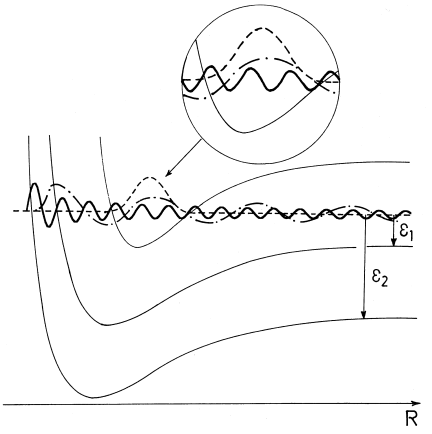

Fig. 5. Visualization of the momentum gap law. The overlap integral (and hence the coupling) between a bound wave function (represented in dashed lines) and that of a pair of fragments is much smaller when the wave function oscillates rapidly because of its high translational momentum (solid line) than when it oscillates gently because of its small momentum (dashed-dotted line). The inset focuses on the region of space where the overlap integral is built up.

5. The momentum gap law

In all of the four reactions studied so far, the appropriate constraint (informative observable) which controls the KERD involves the square root of the translational energy. This observation can be related to the "momentum gap law" which controls the vibrational predissociation dynamics of excited van der Waals complexes [45–48]. According to this law, the couplings that govern the rate of the decay become zero for high values of the relative translational kinetic energy. Therefore, the energy in excess of the thermochemical threshold is preferentially channeled into rotational or vibrational energy of the separating fragments. In other words, only a fraction of the accessible volume in phase space is explored because states with a large translational energy ε are excluded from the sampling of phase space.

In quantum mechanics, this law has a simple interpretation. Predissociation processes should be described in terms of resonances, which are quasi-bound states above the dissociation threshold coupled to the fragmentation channels. In the particular case of a vibrational predissociation, the resonances correspond to a situation where the internal energy is temporarily trapped (e.g. on the microsecond time scale as in mass-spectrometric experimentation) in the vibrational modes other than the reaction coordinate. The resonances are characterized by their lifetime or their associated decay width. An important point is that this width is found to decrease exponentially with the *square root* of the kinetic energy of the fragments, i.e. with the translational momentum [45–47]. It already becomes zero for values of the momentum smaller than the maximal value consistent with the conservation of the total energy. As a result, the final states characterized by a large relative translational momentum do not contribute to the experimentally observed kinetic energy distribution, $\tilde{P}(\varepsilon)$ [48].

The reason for this is that the continuum wave function, i.e. the one for the unbound relative translational motion of the pair of fragments, oscillates with a wavelength that decreases when the translational momentum increases. This behaviour is depicted in Fig. 5, which helps to visualize the overlap between the quasi-bound and the continuum wave functions. In more technical terms, the decay width of a resonant state is proportional to the square of the coupling element, $\langle n|V|\varepsilon\rangle$, between the quasi-bound

wave function, $|n\rangle$, and the isoenergetic state of the continuum, $|\varepsilon\rangle$. The operator V is the coupling responsible for the predissociation process; its explicit form can vary from one kind of predissociation to another. But the important point is that, even if V can be expected to be different for different reaction mechanisms, the momentum gap law derives from the analytical form of the wave function of the continuum, and is therefore expected to apply to a large variety of predissociation processes.

6. Discussion

A comparison between the behaviour of the pyridine ion examined in the present article and that of the halogenobenzene cations previously studied [21,22] raises fundamental questions. In the four examples studied so far, the KERDs, the entropy deficiencies DS, and the fraction of phase space effectively sampled (e^{-DS}) are very similar.

It should first be noted that the two types of reactions involve ions of similar complexities (both containing an aromatic ring) that fragment in the metastable region of the mass spectrometer. Our experimental procedure selects processes occuring in the microsecond time window so that the sampled rate constants and decay widths are about the same for all four reactions. It turns out also that this time window corresponds to similar internal energies for both the halogenobenzene cations and the pyridine cation [34] and therefore the averaging due to the internal energy distribution $T(E)$ is similar, too. From the small $\langle\varepsilon\rangle$ value measured for $C_5H_5N^{\cdot+}$, it can be inferred that the barriers for the isomerization steps, which have to take place somewhere along the reaction path, lie below the dissociation asymptote and play a minor role in the release of kinetic energy on the fragments.

More surprisingly, all of these reactions are controlled by the momentum gap law in spite of conspicuous differences in the underlying physics. Both the rate constant and the KERD depend on long-range forces. Microscopic reversibility introduces a relationship between the rate constant and the cross-section for association of fragments that, in classical mechanics, is related to long-range forces [4–6]. Product energy partitioning depends therefore on the shape of the potential energy surface at large internuclear distances [1].

The leading term in the multipole expansion (i.e. the lowest value of n in the $-R^{-n}$ expansion) is not the same in the four reactions discussed. In the case of the halogenobenzene cations, one has to deal with a simple bond cleavage process along a barrierless reaction path. The long-range forces result from charge-induced-dipole ($-R^{-4}$) and charge-quadrupole ($-R^{-3}$) interactions [22]. By contrast, in the case of the pyridine ion, the long-range forces are expected to involve a charge-permanent dipole ($-R^{-2}$) interaction. However, in that case, the reaction coordinate is not easily defined since the fragmentation must involve a substantial rearrangement including the rupture of an aromatic ring and the eventual formation of a methylene cyclopropene cation [36–43].

What these four reactions have, nevertheless, in common is that the constraint depends on the momentum, i.e. on the square root of the translational energy. As discussed in Sec. 5, even if the coupling operator V differs in the case of the pyridine and the halogenobenzene ions, it is not surprising to observe that the momentum gap law constrains these dissociations, and hence, that very similar shapes are obtained for the KERDs. From a chemical point of view, the reaction mechanisms present obvious differences. However, from a quantum-mechanical point of view, the momentum gap law derives from the analytical form of the wave function of the continuum and applies to a large variety of processes. It would presumably apply equally well to dipolar or quadrupolar long-range interactions.

What has been theoretically analyzed here is the phase space sampled by the pair of fragments, thus at an infinite value of the reaction coordinate. Therefore, the analysis concerns the energy partitioning between the reaction coordinate and the subset of the internal vibrational modes. The simple, structureless shape of the KERD did not allow us to identify more than one dynamical constraint from a comparison between the experimental curve and the calculated prior distributions. The analysis, in all cases studied so far, indicates the action of a systematic effect which prevents

the energy partitioning between the reaction coordinate and the subset of internal modes from being fully statistical. The extent of the discrepancy could be measured; about 25% of the available phase space remain unexplored. Perfect agreement with the experimental KERD can be obtained using this single constraint only, together with an assumption of complete energy randomization within the subset of internal degrees of freedom. Concerning the latter point, however, no information is in fact available and one has to remain noncommittal.

Acknowledgements

We thank Dr. A.J. Lorquet for the calculation of the vibrational frequencies of the $C_4H_4^{\cdot+}$ ion. This work has been supported by a research grant from the Fonds de la Recherche Fondamentale Collective.

References

[1] T. Baer, W.L. Hase, Unimolecular Reaction Dynamics. Theory and Experiments, Oxford University Press, New York, 1996.
[2] W. Forst, Theory of Unimolecular Reactions, Academic, New York, 1973.
[3] C.E. Klots, J. Phys. Chem. 75 (1971) 1526.
[4] C.E. Klots, Z. Naturforsch. 27a (1972) 553.
[5] C.E. Klots, J. Chem. Phys. 58 (1973) 5364.
[6] C.E. Klots, J. Chem. Phys. 64 (1976) 4269.
[7] C.E. Klots, Acc. Chem. Res. 21 (1988) 16.
[8] W.J. Chesnavich, M.T. Bowers, J. Am. Chem. Soc. 99 (1977) 1705.
[9] W.J. Chesnavich, M.T. Bowers, in M.T. Bowers (Ed.), Gas Phase Ion Chemistry, Academic, New York, 1979.
[10] M. Quack, J. Troe, Ber. Bunsenges. Phys. Chem. 78 (1974) 240.
[11] R.D. Levine, R.B. Bernstein, in W.H. Miller (Ed.), Dynamics of Molecular Collisions, Part B, Plenum, New York, 1976.
[12] R.D. Levine, J.L. Kinsey, in R.B. Bernstein (Ed.), Atom-Molecule Collision Theory, Plenum, New York, 1979.
[13] R.D. Levine, Adv. Chem. Phys. 47 (1981) 239.
[14] R.D. Levine, in M. Baer (Ed.), Theory of Chemical Reaction Dynamics, CRC Press, Boca Raton, FL, 1985.
[15] R.D. Levine, R.B. Bernstein, Molecular Reaction Dynamics and Chemical Reactivity, Oxford University Press, New York, 1987.
[16] J.C. Lorquet, Mass Spectrom. Rev. 13 (1994) 233.
[17] C. Lifshitz, J. Phys. Chem. 87 (1983) 2304.
[18] J. Momigny, R. Locht, G. Caprace, Int. J. Mass Spectrom. Ion Phys. 71 (1986) 159.
[19] J. Momigny, R. Locht, Chem. Phys. Lett. 211 (1993) 161.
[20] Y.S. Cho, J.C. Choe, M.S. Kim, J. Phys. Chem. 99 (1995) 8645.
[21] P. Urbain, F. Remacle, B. Leyh, J.C. Lorquet, J. Phys. Chem. 100 (1996) 8003.
[22] P. Urbain, B. Leyh, F. Remacle, A.J. Lorquet, R. Flammang, J.C. Lorquet, J. Chem. Phys. (unpublished).
[23] E. Illenberger, J. Momigny, Gaseous Molecular Ions, Springer-Verlag, New York, 1992.
[24] A. Kafri, Chem. Phys. 13 (1976) 309.
[25] F. Iachello, R.D. Levine, Europhys. Lett. 4 (1987) 389.
[26] R.D. Levine, Adv. Chem. Phys. 70 (1988) 53.
[27] M. Barber, R.M. Elliot, 12th Annual Conference on Mass Spectrometry and Allied Topics, Montreal, 1964.
[28] S. Harakawa, M. Yoshioka, T. Sugiura, Int. J. Mass Spectrom. Ion Processes 87 (1989) 309.
[29] J.L. Holmes, A.D. Osborne, Int. J. Mass Spectrom. Ion Phys. 23 (1977) 189.
[30] R.G. Cooks, J.H. Beynon, R.M. Caprioli, G.R. Lester, Metastable Ions, Elsevier, Amsterdam, 1973.
[31] J.H. Beynon, A.E. Fontaine, G.R. Lester, Int. J. Mass Spectrom. Ion Phys. 8 (1972) 341.
[32] J.H. Eland, J. Berkowitz, H. Schulte, R. Frey, Int. J. Mass Spectrom. Ion Phys. 28 (1978) 297.
[33] H.M. Rosenstock, R. Stockbauer, A.C. Parr, Int. J. Mass Spectrom. Ion Phys. 38 (1981) 323.
[34] P.C. Burgers, J.L. Holmes, Int. J. Mass Spectrom. Ion Processes 58 (1984) 15.
[35] S.E. Stein, B.S. Rabinovitch, J. Chem. Phys. 58 (1973) 2438.
[36] T. Baer, G.D. Willet, D. Smith, J.S. Phillips, J. Chem. Phys. 70 (1979) 4076.
[37] C. Lifshitz, D. Gibson, K. Levsen, I. Dotan, Int. J. Mass Spectrom. Ion Phys. 40 (1981) 157.
[38] P. Ausloos, J. Am. Chem. Soc. 103 (1981) 3931.
[39] W. Wagner-Redeker, A.J. Illies, P.R. Kemper, M.T. Bowers, J. Am. Chem. Soc. 105 (1983) 5719.
[40] E. Weger, W. Wagner-Redeker, K. Levsen, Int. J. Mass Spectrom. Ion Phys. 47 (1983) 77.
[41] W.J. Van der Hart, Org. Mass Spectrom. 23 (1988) 187.
[42] M.-Y. Zhang, C. Wesdemiotis, M. Marchetti, P.O. Danis, J.J.C. Ray, B.K. Carpenter, F.W. McLafferty, J. Am. Chem. Soc. 111 (1989) 8341.
[43] S.W. Staley, T.D. Norden, J. Am. Chem. Soc. 111 (1989) 445.
[44] M.J. Frisch, G.W. Trucks, H.B. Schlegel, P.M.W. Gill, B.G. Johnson, M.A. Robb, J.R. Cheeseman, T. Keith, G.A. Petersson, J.A. Montgomery, K. Raghavachari, M.A. Al-Laham, V.G. Zakrzewski, J.V. Ortiz, J.B. Foresman, C.Y. Peng, P.Y. Ayala, W. Chen, M.W. Wong, J.L. Andres, E.S. Replogle, R. Gomperts, R.L. Martin, D.J. Fox, J.S. Binkley, D.J. Defrees, J. Baker, J.P. Stewart, M. Head-Gordon, C. Gonzalez, J.A. Pople, GAUSSIAN 94, Revision B.3, Gaussian, Inc., Pittsburgh, 1995.
[45] G.E. Ewing, J. Chem. Phys. 71 (1979) 3143.
[46] G.E. Ewing, J. Chem. Phys. 72 (1980) 2096.
[47] J.A. Beswick, J. Jortner, Adv. Chem. Phys. 47 (1981) 363.
[48] M. Desouter-Lecomte, J. Liévin, V. Brems, J. Chem. Phys. 103 (1995) 4524.